Overcoming temporal polarization instabilities from the latent birefringence in all-normal dispersion, wave-breaking-extended nonlinear fiber supercontinuum generation

Scott R. Domingue[1,*] and Randy A. Bartels[1,2]

[1]*Department of Electrical and Computer Engineering, Colorado State University, Fort Collins, CO 80523, USA*

[2]*School of Biomedical Engineering, Colorado State University, Fort Collins, CO 80523, USA*

[*]*domingue@rams.colostate.edu*

Abstract: The intrinsic weak birefringence in all-normal dispersion highly nonlinear fiber, particularly ultra-high-numerical-aperture fiber, generates supercontinuum with long term polarization instabilities, even for seed pulses launched along the perceived slow axis of the fiber. Highly co/anti-correlated fluctuations in energy between regions of power spectral density mask the extent of the spectral noise in total integrated power measurements. The instability exhibits a seed pulse power threshold above which the output polarization state of the supercontinuum seeds from noise. Eliminating this instability through the utilization of nonlinear fiber with a large designed birefringence, encourages the exploration of compression schemes and seed sources. Here, we include an analysis of the difficulties for seeding supercontinuum with the highly attractive ANDi-type lasers. Lastly, we introduce an intuitive approach for understanding supercontinuum development and evolution. By modifying the traditional characteristic dispersion and nonlinear lengths to track pulse properties within the nonlinear fiber, we find simple, descriptive handles for supercontinuum evolution.

OCIS codes: (060.2420) Fibers, polarization-maintaining; (190.4370) Nonlinear optics, fibers; (320.5520) Pulse compression; (320.6629) Supercontinuum generation.

References and links

1. J. M. Dudley, G. Genty, and S. Coen, "Supercontinuum generation in photonic crystal fiber," Rev. Mod. Phys. **78**, 1135–1184 (2006).
2. A. Heidt, J. Rothhardt, A. Hartung, H. Bartelt, E. Rohwer, J. Limpert, and A. Tnnermann, "High quality sub-two cycle pulses from compression of supercontinuum generated in all-normal dispersion photonic crystal fiber," Opt. Express **19**, 13873–13879 (2011).
3. A. Heidt, A. Hartung, G. Bosman, P. Krok, E. Rohwer, H. Schwoerer, and H. Bartelt, "Coherent octave spanning near-infrared and visible supercontinuum generation in all-normal dispersion photonic crystal fibers," Opt. Express **19**, 3775–3787 (2011).
4. P. Champert, V. Couderc, P. Leproux, S. Fvrier, V. Tombelaine, L. Labont, P. Roy, C. Froehly, and P. Nrin, "White-light supercontinuum generation in normally dispersive optical fiber using original multi-wavelength pumping system," Opt. Express **12**, 4366–4371 (2004).

#179077 - $15.00 USD Received 1 Nov 2012; accepted 2 May 2013; published 24 May 2013

5. L. Hooper, P. Mosley, A. Muir, W. Wadsworth, and J. Knight, "Coherent supercontinuum generation in photonic crystal fiber with all-normal group velocity dispersion," Opt. Express **19**, 4902–4907 (2011).
6. H. Tu, Y. Liu, X. Liu, D. Turchinovich, J. Lgsgaard, and S. Boppart, "Nonlinear polarization dynamics in a weakly birefringent all-normal dispersion photonic crystal fiber: toward a practical coherent fiber supercontinuum laser," Opt. Express **20**, 1113–1128 (2012).
7. Y. Liu, H. Tu, and S. Boppart, "Wave-breaking-extended fiber supercontinuum generation for high compression ratio transform-limited pulse compression," Opt. Lett. **37**, 2172–2174 (2012).
8. D. L. Marks, A. L. Oldenburg, J. J. Reynolds, and S. A. Boppart, "Study of an ultrahigh-numerical-aperture fiber continuum generation source for optical coherence tomography," Opt. Lett. **27**, 2010–2012 (2007).
9. H. G. Winful, "Self-induced polarization changes in birefringent optical fiber," Appl. Phys. Lett. **47**, 213–215 (1986).
10. S. Wabnitz, "Modulation polarization instability of light in a nonlinear birefringent dispersive medium," Phys. Rev. A **38**, 2018–2021 (1988).
11. Z. Zhu and T. Brown, "Polarization properties of supercontinuum spectra generated in birefringent photonic crystal fibers," J. Opt. Soc. Am. B **21**, 249–257 (2004).
12. A. Chong, J. Buckley, W. Renninger, and F. Wise, "All-normal-dispersion femtosecond fiber laser," Opt. Express **14**, 10095–10100 (2006).
13. C. Finot, B. Kibler, L. Provost, and S. Wabnitz, "Beneficial impact of wave-breaking for coherent continuum formation in normally dispersive nonlinear fibers," J. Opt. Soc. Am. B **25**, 1938-1948 (2008).
14. R. W. Boyd, *Nonlinear Optics* (Academic, NY, 2003).
15. G. Clay, A. Millard, C. Schaffer, J. Aus-der-Au, P. Tsai, J. Squier, and D. Kleinfeld, "Spectroscopy of third-harmonic generation: evidence for resonances in model compounds and ligated hemoglobin," J. Opt. Soc. Am. B **23**, 932–950 (2006).
16. D. J. Kane, "Principal components generalized projections," J. Opt. Soc. Am. B **25**, A120–A132 (2008).
17. H. Tu, D. Marks, Y. Koh, and S. Boppart, "Stabilization of continuum generation from normally dispersive nonlinear optical fibers for a tunable broad bandwidth source for optical coherence tomography," Opt. Lett. **32**, 2037–2039 (2007).
18. S. Murdoch, R. Leonhardt, and J. Harvey, "Polarization modulation instability in weakly birefringent fibers," Opt. Lett. **20**, 866–868 (1995).
19. J. Wilson, P. Schlup, and R. Bartels, "Ultrafast phase and amplitude pulse shaping with a single, one-dimensional, high-resolution phase mask," Opt. Express **15**, 8979–8987 (2007).

1. Introduction

SuperContinuum (SC) generation in the normal dispersion regime has attracted intense interest due to preservation of the seed laser's coherence. The principal effort in SC generation has been focused on anomalous dispersion fibers with low net dispersion. While these fibers generate substantial spectral widths, they suffer from de-coherence mechanisms, such as modulation instability that are not allowed in a normal dispersion regime. Preserving coherence in anomalous dispersion SC generation requires extremely short fiber lengths and launching with short input laser pulses [1]. Fibers exhibiting normal dispersion relax the constraints on the launched pulse duration, and permit stable SC generation with a much broader range of input pulse parameters. Photonic crystal fibers (PCF) with all normal dispersion have been used to create few-cycle pulses [2], octave-spanning SC [3], white-light SC [3, 4], and high compression ratio pulses [2, 5–7]. Solid, ultrahigh-numerical-apertures (UHNA) fibers with all normal dispersion profiles are less frequently used, e.g. generating SC for optical coherence tomography [8]. However, all normal dispersion UHNA fibers are an attractive source for generating SC since they are low cost, relatively easy to splice to other fibers, and can be directly connectorized.

We present the discovery that SC generation in all normal dispersion UHNA fibers displays a launch power threshold, beyond which the SC is incoherent. The level of noise is highly dependent on the launch polarization, indicating even for non-polarization maintaining (PM) fiber the weak, residual stress birefringence plays a critical role in the evolution of SC with propagation. The SC incoherence traces back to a polarization instability driven by this weak intrinsic birefringence in otherwise single mode fibers. Above threshold, polarization modulation instability corrupts the spectral composition of the principal output polarization through energy coupling between the orthogonal polarization modes, even for seed pulses oriented along the effective

#179077 - $15.00 USD Received 1 Nov 2012; accepted 2 May 2013; published 24 May 2013

slow axis of the nonlinear fiber. A combination of low level laser noise and quantum noise from the orthogonal polarization state results in the continuous random fluctuation of the SC output polarization state. Polarization dynamics in birefringent fiber with pulses launched in the all normal dispersion regime have been widely reported [6, 9–11] however, the reported dynamics primarily deal with the stable coupling of power into spectral sidebands.

Additionally, we observe an instability on long time-scales consistent with thermalization. This suggests that slight temperature drifts change the fiber stresses and perturb the fiber polarization axes, leading to a drift in the polarization state at the fiber output. Moreover, we note that this SC polarization instability produces noise that is highly correlated spectrally. In fact, without observing the spectrally-resolved power spectral density fluctuations, the correlated spectral noise averages out in a polarized total power measurement of the SC pulse train leading to a severe underestimation of the total noise.

The optimal solution for generating stable SC in the all normal dispersion regime is PM nonlinear fibers. We describe a spliced fiber cocktail for easy and efficient coupling of seed pulses into the nonlinear PM fiber. SC generated by this fiber system exhibit spectral stability comparable to that of the oscillator seed pulse. The SC were compressed to nearly transform-limited $\sim$ 38-fs pulses with the combination of a phase-only pulse shaper cascaded with a transmission grating compressor to remove the large fiber group delay dispersion (GDD). The $9\times$ compression ratio represents the first to our knowledge demonstration of nonlinear pulse compression from non-PCF, highly dispersive, all normal dispersion nonlinear fiber.

The noise and spectral broadening properties of SC seeded with an ANDi-type Yb-doped fiber laser [12] are also investigated. ANDi lasers offer an attractive alternative to bulk Yb-doped soliton modelocked oscillators due to the favorable energy and bandwidth scaling properties of the dissipative-soliton modelocking mechanism in addition to their low cost, ease of alignment, and high-quality beam spatial profile. However, the structure of the power spectrum and the complexity of the oscillator's spectral phase perturbs the nonlinear pulse propagation, leading to SC generation characteristics that are qualitatively and quantitatively distinct from spectra generated by seed pulses from soliton-like modelocking with near-zero net intracavity GDD.

While the nonlinear fiber propagation characteristics are strongly dependent on the pulse launch parameters such as the power spectrum and pulse chirp at the fiber input, we introduce new parameters that track local and cumulative pulse propagation dynamics. These parameters provide a universal approach to optimizing the SC for particular target application goals. We implemented a split step fiber propagator using the generalized nonlinear schrdinger equation (GNLSE) [1] to model and design the nonlinear fiber cocktails. With the numerical model, we find excellent agreement between theory and experiment, and also validate our universal scaling parameters. This model is then used to explore SC generation over a wide range of the launch pulse parameter space. Surprising regions are found that relax constraints on fiber design tolerances for applications involving large peak power generation for driving nonlinear optical signals.

2. Spectral phase evolution

Applications where a compressed or shaped laser pulse are desired, the spectral phase of the SC spectrum, its stability, and complexity are critical issues. Here, we study the spectral phase complexity, spectral smoothness, and pulse compressibility in the normal dispersion regime under a wide range of pulse launch parameters by numerical integration of the GNLSE with a split-step propagator. Given that we have found experimentally that PM fibers preserve SC polarization to a large degree, we only implement the GNLSE for a single eigen polarization of the fiber system. As a reference point, we assume fiber launch conditions that mimic our

#179077 - $15.00 USD Received 1 Nov 2012; accepted 2 May 2013; published 24 May 2013

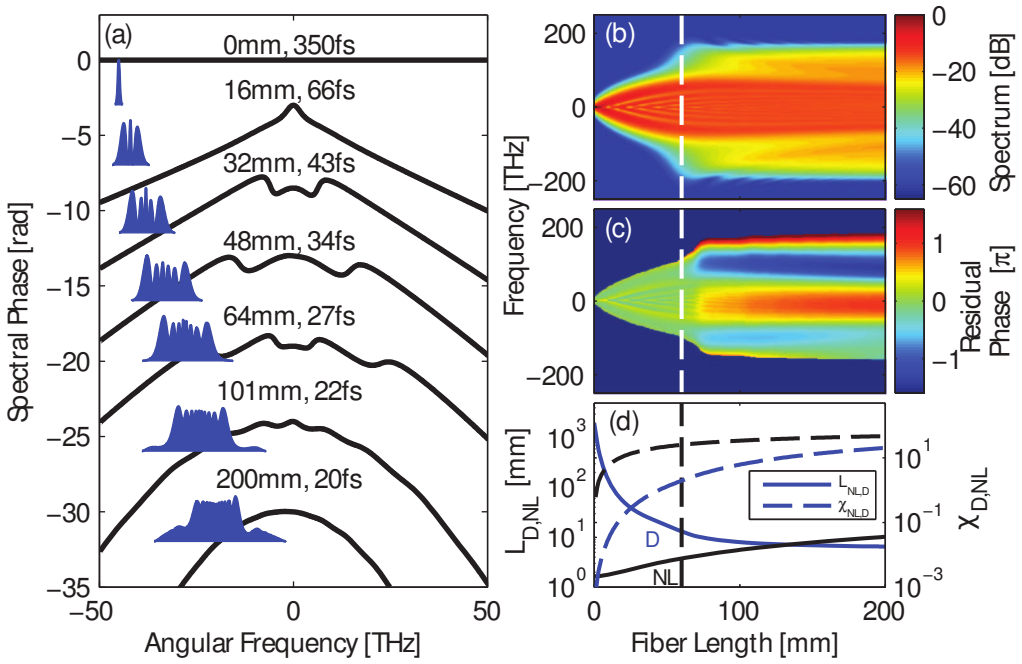

Fig. 1. (a) SC spectral phase from 4 nJ 350 fs seed pulses for different fiber lengths with the transform limit and power spectrum inset. Evolution of the (b) power spectrum (c) residual spectral phase after GDD compensation (residual phase set to -5 outside of the -20 dB power spectral envelope) and (d) local and accumulated characteristic lengths all as a function of fiber length. The local dispersion length and accumulated dispersion lengths, χ_D, are in blue and the local nonlinear length and accumulated nonlinear length, χ_{NL}, are in black. The calculated length for the onset of WB, 62 mm, is included as the vertical dashed white line in (b) and (c) and dashed black line in (d)

experiments described later in the paper: 350 fs hyperbolic secant (sech) seed pulses at 1027 nm, 4 nJ of energy coupled into the nonlinear fiber (or 284 mW at 71 MHz), and Nufern UHNA-3 nonlinear fiber. The parameter space in a region around this operating point is explored, providing guidance for the expected behavior over a wide range of ultrafast modelocked laser operating parameters.

The spectral phase (and power spectra as an inset) of the SC spectrum for the pulse energy and bandwidth matching the characteristics from our oscillator for fiber lengths up to and beyond optical wave breaking (WB) are shown in Fig. 1(a). The onset of WB for our example nonlinear system is $z_{WB} = 62$ mm. This quantity is based on a definition of WB where new instantaneous frequencies, generated by self phase modulation (SPM), temporally overlap with different instantaneous frequencies from the central bandwidth due to propagation in the presence of group delay dispersion (GDD). The resulting intensity beating is referred to as WB, for which a distance can be computed from the expression [13].

$$z_{WB} = \frac{L_D(z=0)}{\sqrt{4\exp(-3/2)N^2 - 1}} \tag{1}$$

Here, $L_D(z=0)$ is the dispersion length determined by the bandwidth of the incident seed pulse coupled into the fiber and N is the soliton number of the seed pulse.

The sinusoidal beating in the pulse's intensity following WB initiates four wave mixing

#179077 - $15.00 USD Received 1 Nov 2012; accepted 2 May 2013; published 24 May 2013

(FWM). The spectral phase and envelope modulations characteristic of SPM dominated SC evolution, as seen in Fig. 1(a) for fiber lengths < 62 mm, are smoothed out by the subsequent FWM [13]. In addition to the reduction of phase and amplitude structure, FWM generates long spectral tails that further drive down the transform limit of the pulse supported by the SC spectrum. These spectral tails are slow growing however, since they are a product of WB and, therefore, a diminished pulse peak power. Figure 1(b) illustrates the sudden appearance of these WB/FWM spectral tails after WB, white dashed-line at z_{WB}. In our example system, the SC's transform limit decreases from 28 fs at the onset of WB to 17 fs at a 1000 mm fiber length due to this additional bandwidth from WB/FWM.

The large, but smooth, variation in group delay associated with the spectral phase structure post-WB suggests a simple temporal pulse compressor might be sufficient. Counter intuitively, the pre-WB SPM phase structure barely inhibits a simple compression system from reaching near transform limited pulses, due partly to the correlation of the spectral phase structure to power spectral nulls. Figure 1(c) plots the simulated residual spectral phase following only GDD compensation as a function of fiber length. Propagation significantly past the WB threshold makes pulse compression acutely more difficult, as seen in the rapid accumulation of residual phase beyond the white dashed line denoting the onset of WB in Fig. 1(c).

To help explain this spectral phase evolution, we introduce the concept of local characteristic lengths – the spatially (longitudinally) evolving compliments of the common dispersion and nonlinear lengths which are based on the initial launch conditions. We define the local dispersion and nonlinear lengths as

$$L_{\mathrm{D}}(z) = \frac{\tau(z)^2}{|\beta_2|}, \qquad L_{\mathrm{NL}}(z) = \frac{1}{\gamma_0 P(z)} \tag{2}$$

where z is the local fiber position, $\tau(z)$ is the full-width-half-max (FWHM) of the transform limited pulse duration supported by the SC bandwidth, β_2 is the group velocity dispersion of the nonlinear fiber, γ_0 is the nonlinear coefficient, and $P(z)$ is the peak power. The local characteristic lengths for the example system are plotted in Fig. 1(d). The local dispersion length undergoes the more dramatic change falling from 1.9 m at the input to < 10 mm after 200 mm of propagation. The falling local dispersion length is simply a reflection of the shortening transform limited pulse duration supported by the broadening power spectrum. The local nonlinear length increases due to a drop in the peak power of the pulse from the temporal pulse stretching that occurs with fiber propagation, e.g. at the onset of WB the peak power has fallen by a $\frac{1}{2}$, as reported in Ref [13], and the local nonlinear length increases by a factor of 2.

In addition to the local characteristic lengths, we also introduce a parameter for the accumulated amount of each local length: $\chi_i(z) = \int_0^z 1/L_i(z')\mathrm{d}z'$, where $i = \mathrm{D}, \mathrm{NL}$. These parameters are referred to as the accumulated dispersion and nonlinearity for $i =$D and $i =$NL, respectively. The accumulated nonlinear length is analogous to the B-integral. The interpretation of either of the accumulated quantities is taken from the static, initial characteristic lengths: at $\chi_{\mathrm{D}}(z') = 1$ the temporal duration will have chirped out to $\tau(z') = \sqrt{2}\tau_0$ and at $\chi_{\mathrm{NL}}(z'') = 1$ the power spectrum will have increased to $\Delta\Omega(z'') = \sqrt{2}\Delta\Omega_0$.

Using these new metrics we re-examine the problem of SC compressibility as a function of fiber propagation. Prior to WB, the SPM generated spectra has not meaningfully sampled the complexity of the fiber dispersion. The fast initial rate of change in the accumulated dispersion in Fig. 1(d) reflects the plummeting local dispersion length, but does not introduce significant chirp since the accumulated dispersion is still very small. The accumulated dispersion at the onset of WB is not only low, $\chi_{\mathrm{D}}(z_{\mathrm{WB}}) \sim 2$, but it also contains the accumulation of dispersion for the narrower initial spectral bandwidths. At WB however, the local dispersion length has become quite short, 13 mm in our particular example. Propagation beyond this point results in

#179077 - $15.00 USD Received 1 Nov 2012; accepted 2 May 2013; published 24 May 2013

the rapid accumulation of spectral phase with significant higher order dispersion (HOD), due to the short local dispersion length and (now) broad spectra. To reach the shorter transform limited pulses that accompany propagation past WB, a pulse shaper is required to compensate the HOD.

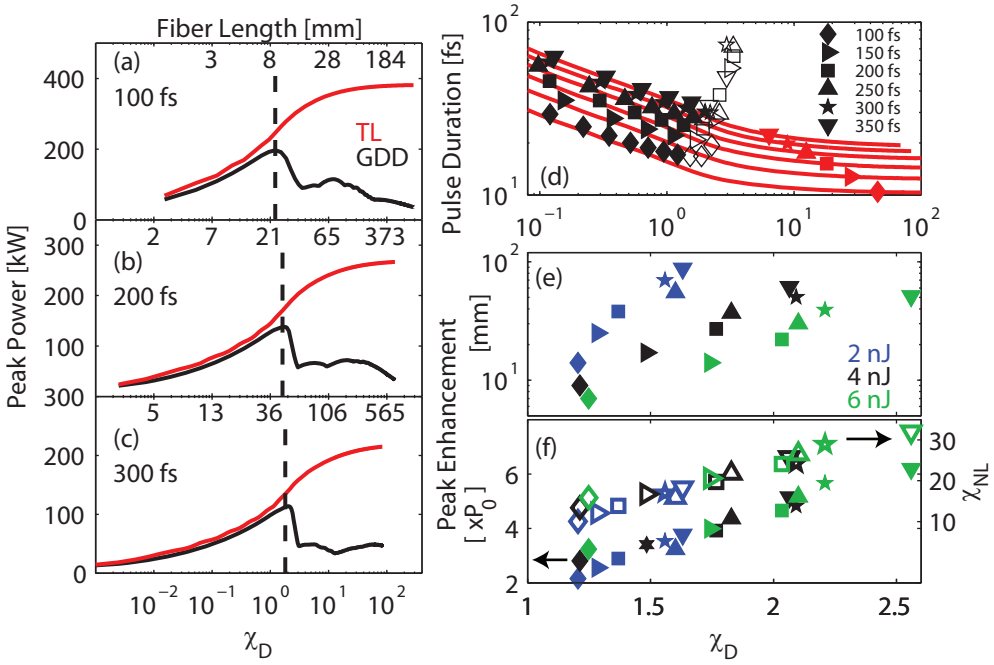

Fig. 2. The peak power evolution with χ_D for 4 nJ 100 fs (a), 200 fs (b), and 300 fs (c) seed pulses and GDD compensation in black and complete compensation to the transform limit in red. The onset of WB is plotted in (a)-(c) as a dashed vertical line. (d) The transform limited pulse duration in red and the pulse duration with only GDD compensation in black markers as functions of χ_D for 4 nJ pulses and a suite of seed pulse durations: 100 - 350 fs. The solid black markers indicate the evolution up to the maximum peak power enhancement with GDD compensation, followed by hollow markers for additional propagation. The fiber length corresponding to the maximum peak power enhancement with GDD compensation as a function of χ_D (e) for a suite of seed pulses: 2, 4, and 6 nJ shown in blue, black, and green respectively, and pulse durations from 100-350 fs. The maximum peak power enhancement factor with GDD compensation, relative to the incident seed pulses (composed of twice the energy), and the accumulated nonlinear length at peak enhancement(f).

Moving from the narrow focus of our example nonlinear system to a broader parameter space, we expand our analysis on the evolving SC. Across a whole suite of seed pulses (energies of 2, 4, and 6 nJ and pulse durations of 100-350 fs), it is always the case that around the onset of WB, simple compression systems fail to compensate the HOD; resulting in a highly structured intensity envelope. Figures 2(a)-2(c) shows the transform limited and GDD compensated SC peak powers from 4 nJ seed pulses with 100, 200, and 300 fs pulse durations respectively, as functions of accumulated dispersion. For simplicity, these and the following peak power calculations neglect compressor losses. Propagation beyond WB causes the broad bandwidth to accumulate fiber dispersion over a larger range, with the spectral phase accumulating significant HOD. The peak power cliff-fall in the black GDD compensation curves of Figs. 2(a)-2(c), corresponds to the accumulation of enough HOD following WB, to reduce the intensity from a

#179077 - $15.00 USD Received 1 Nov 2012; accepted 2 May 2013; published 24 May 2013

simple compressor.

The point where the GDD compensated peak power reaches a maximum before the cliff-fall, which we will refer to as the peak enhancement, is a critical quantity for practical applications and is plotted in Figs. 2(d)-2(f). Even though the cliff-edge varies across this parameter space over an order of magnitude in fiber lengths, it peaks very close to the individual WB lengths and in a small region of accumulated dispersion. The hollow markers of Fig. 2(d) represent propagation beyond the peak enhancement and are tightly congregated between $1 < \chi_D < 2$. A trend of hastening the peak enhancement arrival with falling seed pulse duration begins to manifest itself in Fig. 2(d).

The slope and shape of the cliff-fall is highly dependent on the incident seed pulse. At longer duration seed pulses, the GDD compensated peak power has very sharp enhancement peak. For shorter duration seed pulses however, the GDD compensated peak power begins to diverge from the transform limited peak power prior to the onset of WB. This results in the rounding of the peak, seen in Fig. 2(a), and is a consequence of the increased sensitivity of the shorter incident seed pulse to HOD. The heightened sensitivity to HOD for shorter seed pulses is maintained with seed energy, as seen in Fig. 2(e) where the peak enhancement arrives at smaller accumulated dispersion lengths for shorter seed pulse durations.

Figure 2(f) plots the peak power enhancement with GDD-limited spectral phase compensation, relative to the incident seed pulse peak power and the accumulated nonlinearity at peak enhancement. Here, we assume a total transmission efficiency of 50% including the fiber coupling, fiber launch, and compressor efficiencies. The incident seed energy then, is taken to have twice the energy of the GDD compensated SC pulse, giving a strict comparison of peak power enhancement. The SC with the largest accumulated dispersion length at the peak enhancement also has the largest relative peak power enhancement, as seen in the solid markers of Fig. 2(f). The larger accumulated dispersion at peak enhancement is accompanied with a larger accumulated nonlinearity, shown in the hollow markers of Fig. 2(f). The ratio of GDD compensated SC duration to seed pulse duration increases with seed pulse duration, as expected from the increasing accumulated nonlinearity with seed pulse duration.

The previous discussion assumed the luxury of arbitrary fiber lengths. But, it is possible that for particular applications the optimal fiber length is impractically small for connectorizing, splicing, etc. (e.g. the 100 fs, 6 nJ seed pulse in UHNA-3 fiber with a peak enhancement at 8 mm, shown as the green diamonds in Figs. 2(e) and 2(f)). Rather than reducing the seed power to raise the peak enhancement position to a practical length, we provide an alternate solution that keeps the seed power high and relaxes the short fiber requirements for simple compression. An interesting consequence of this work is the realization of the novel gains available from third order dispersion (TOD) compensation. We find that while the GDD and TOD compensated SC peak power still undergoes a cliff-fall after a primary enhancement peak, with the addition of TOD compensation there is a secondary maximum, shown in the green curve of Fig. 3(a). The secondary peak enhancement is due to the specific shape of the UHNA dispersion. The secondary peak enhancement is also only seen for the shorter duration seed pulses.

The inset Figs. in Fig. 3(a) show the progression in compressed SC intensity from the primary peak enhancement, Fig. 3(a1), to the bottom of the cliff-fall, Fig. 3(a2), to the secondary peak enhancement, Fig. 3(a3), and finally at the secondary peak enhancement position with only GDD compensation, Fig. 3(a4). Relative to the SC at the primary peak enhancement position, the SC at the secondary peak enhancement has more bandwidth. TOD and GDD compensation is sufficient to produce a pulse with a central temporal lobe shorter in duration than attainable at the primary peak enhancement but with side lobes from quadratic chirp. The two major potential benefits are: 1) the location of the secondary peak enhancement is shifted to an achievable fiber length (51 mm as opposed to 8 mm) and 2) the broadening of the peak enhancement

#179077 - $15.00 USD Received 1 Nov 2012; accepted 2 May 2013; published 24 May 2013

curve. With only GDD compensation, the peak enhancement requires fiber length precisions of < 1 mm, whereas the secondary enhancement with GDD and TOD relaxes this precision requirement to 1 cm.

As convenient metrics of utility, we supplement the peak power computations with the total second harmonic generation (SHG) signal [14] and total third harmonic generation (THG) signal [15] expected from SC seeded with 100 fs 6 nJ pulses compressed with various orders of compensation, assuming samples thin enough to neglect phase-matching. The harmonic signals plotted in Fig. 3(b) are normalized to the signal expected from the seed pulse incident on the fiber (where again we are assuming a total efficiency of 50% so the normalization is based on a 12 nJ pulse). The primary GDD compensated peak enhancement, for this particular seed pulse, yields a 1.5 and 5.3 fold improvement in the SHG and THG signals respectively. The secondary peak enhancement harmonic improvements are more modest, but still a respectable 1.3 and 4.5 for SHG and THG respectively. For comparison, towards the opposite end of the seed duration/energy spectrum, the pulses simulating our Yb:KYW oscillator of 350 fs and 4 nJ seed pulses yield improvements of 3.2 and 21 for SHG and THG, respectively with GDD compensation of the primary enhancement. These enhancements are potentially artificially low, since any measurement with average power limitations requiring power attenuation (e.g. interrogating a biological sample with a tightly focused beam) will drive up the relative enhancement factors of the compressed SC.

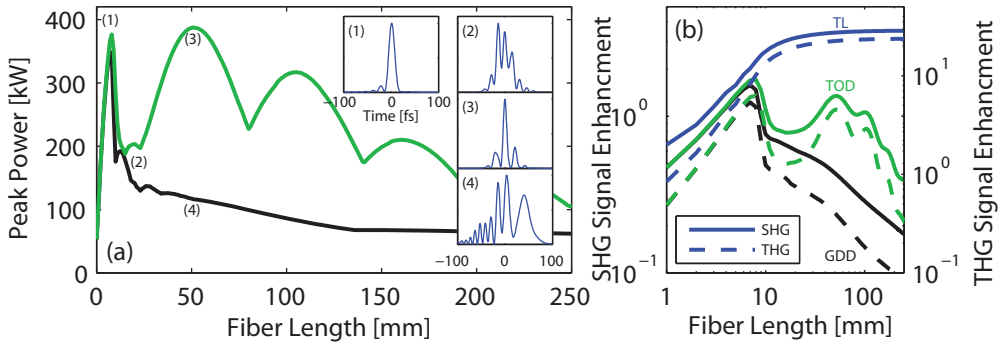

Fig. 3. (a) The peak power evolution as a function of fiber length for 6 nJ 100 fs seed pulses with GDD compensation in black and GDD and TOD compensation in green. The compressed SC intensity is shown at several fiber lengths and compensation orders in inset Figs. (a1)-(a4). The SHG and THG signal enhancement relative to the incident 12 nJ 100 fs pulse, as a function of fiber length and order of compensation: transform limited in blue, GDD and TOD in green, and GDD in black.

3. Birefringent nonlinear fiber

End coupling is often used to launch laser pulses into PCF and high NA fibers, which is subject to optical degradation of the end face and coupling drift due to tight coupling tolerances on beam size and alignment. These sensitivities and damage mechanisms lead to challenges for long-term stable operation of SC fiber sources. To avoid end-coupling into high NA fibers as well as to improve the long-term experimental stability, we have designed a fiber cocktail system that provides long term coupling stability in addition to ease of implementation. Splicing UHNA fiber to standard optical fiber (~ 7 micron core), leverages the ease of coupling pulses

#179077 - $15.00 USD Received 1 Nov 2012; accepted 2 May 2013; published 24 May 2013

into standard fiber using a commercially available aspheric collimator and an APC connector to easily, efficiently, and robustly get light into the UHNA fiber. We connectorize the fiber cocktail to keep the entrance fiber (the standard fiber) short (5-10 mm). Splices between the standard fiber and UHNA fiber are robust and relatively low loss (-1.4 dB). The total coupling efficiency into the nonlinear fiber is typically 50% (depending on the fiber cocktail), which is comparable or better than typical reported coupling efficiencies using objectives (or aspheres) and bare fibers [8]. The connector/collimator unit also serves to protect the fiber face as well as minimizing coupling loss due to fiber drift. For applications involving short pulse compression, the output would ideally be directly from the nonlinear fiber, connectorized and collimated by a commercially available aspheric collimator or off-axis parabolic mirror collimator.

The previous discussion regarding SC generation in the normal dispersion regime assumes fibers with *zero* birefringence. In real fibers, this is an unattainable ideality. As a result, even non-PM fibers exhibit a weak birefringence that can drive polarization instability that will decohere and depolarize the generated SC. We discuss the limiting cases of both extremely weak (intrinsic stress-induced) and high (designed) fiber birefringence. We also note that the weak case of birefringence is also extremely sensitive to small environmental perturbations that drive significant drift of the birefringence and present a significant barrier to long-term reliable operation of the SC source.

3.1. Weakly birefringent nonlinear fiber

The simplest system studied employed a high NA, single mode fiber Nufern UHNA-3. This fiber is both all normally dispersive and highly nonlinear in our spectral operating region. Comparing UHNA-3 to NKT's PCF NL-1050-NEG1, UHNA-3's GDD is 10× greater (-110 ps/nm-km) at 1050 nm, 10× cheaper, and has comparable mode field diameters at 1050 nm. The fiber cocktail started with a $\sim$ 1 cm length of 1060XP (Nufern) fiber for connecting to the collimator, 1 m of UHNA-3 nonlinear fiber, and then 50 cm of 1060XP exit fiber. The total coupled power efficiency through the fiber is 50%, the splice loss between the nonlinear fiber and the exit fiber is much lower than the entrance splice at -0.3 dB. We use 350 fs transform-limited pulses, generated by a Yb:KYW modelocked oscillator, to seed the fiber cocktail, with a center wavelength of 1027 nm and a power spectrum closely approximating a sech distribution, a repetition rate of 71 MHz, and up to 375 mW of average power coupled into the nonlinear fiber.

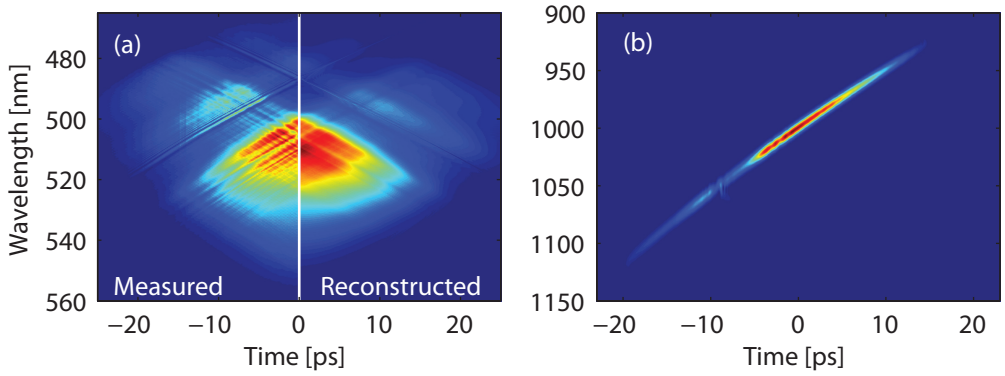

Fig. 4. (a) Phantom SHG-FROG and (b) reconstructed spectrogram

We characterized the SC directly out of the fiber using second harmonic generation fre-

#179077 - $15.00 USD Received 1 Nov 2012; accepted 2 May 2013; published 24 May 2013

quency resolved optical gating (SHG-FROG) and the principal component generalized projection (PCGP) algorithm, which permits the reconstruction of large FROG traces [16]. The large time bandwidth product of the pulse reconstruction required a large vector map to enclose the highly chirped SC ($2^{13} \times 2^{13}$ for the SHG-FROG presented in Fig. 4). SHG-FROG traces obtained from unstable laser pulse trains exhibiting stochastic fluctuations in pulse properties does not converge to a unique, low-error FROG reconstruction. Consequentially, reliable FROG reconstructions are a strong indicator of the stability of the ultrafast laser pulse train. The SHG-FROG trace in Fig. 4 was captured for SC pulses generated by 200 mW average power coupled through the UHNA-3 fiber cocktail. The scanning FROG measurement required roughly half an hour to acquire, and its low FROG-error of 0.04 demonstrates the stability of this particular nonlinear broadening system. The described fiber system however, suffered from an unanticipated spectral instability power threshold.

We found experimentally that stable SC were only generated with coupled average powers beneath 200 mw. Figure 5(a) shows a power spectrum time series of stable SC (comparable to the SC shown in Fig 4). Larger coupled powers led to a destabilization of the SC making it unusable as a practical source, see Figs. 5(a)-5(c) for a progression from stable to unstable SC time series.

It is known that in weakly birefringent fiber, polarization modulation instability can lead to coupling between the effective orthogonal polarization modes of the fiber [6, 9–11]. The stability of SC from weakly birefringent fibers is maximized by launching with a pulse polarization orientation that coincides with the highest preserved polarized output power. This corresponds to overlapping the launch polarization with the effective slow axis of the intrinsic, stress-induced birefringence of the fiber. Experimentally, the launch polarization orientation is found by launching at low power and tuning a half waveplate on the fiber launch side and a combination of half and quarter waveplates preceding a polarizer on the collection side of the fiber. To determine the fast axis from the slow axis, we then measured the spectral noise and designated the axis with lower noise the slow axis.

The spectrally resolved noise in the SC power spectrum was measured using an Andor Shamrock spectrometer and Andor iDus detector. Spectra were acquired at 20-100 Hz rates for time intervals ranging from 45-300 minutes. To ensure that this sampling bandwidth fully captured the noise spectrum of the SC de-coherence and depolarization, relative intensity noise (RIN) measurements of the polarized output SC were captured with a photodiode placed at the focal plane of a spectrometer. The RIN measurements demonstrated that the noise spectrum was limited to < 20 Hz.

We define the depolarization as the fraction of the power coupled into the polarization mode orthogonal to the launch polarization: $P_\perp/(P_\perp + P_\parallel)$, where $P_\parallel$ is the launch polarization. The amount of depolarization is a rapid indicator of the stability of the SC power spectrum. We introduce a metric that we define as the relative spectral noise: $\mathrm{RSN}(\lambda) = \sigma(\lambda)/\mu(\lambda)$, where $\sigma(\lambda)$ is the root mean squared noise over a time series of a spectral bin $\Delta\lambda = 0.5$ nm located at λ and $\mu(\lambda)$ is the mean over the same time interval. The RSN is the spectrally resolved version of the more typical root mean squared noise (RMS-N) – which we will exclusively use in reference to the the standard deviation of the total power fluctuations. We also calculate a total spectral noise metric,

$$\Phi_{\mathrm{RSN}} = \frac{\int \sigma(\lambda)\mu(\lambda)\mathrm{d}\lambda}{\int \mu^2(\lambda)\mathrm{d}\lambda} \tag{3}$$

for comparison to the RMS-N.

At low power, 200 mW, the depolarization is 25%, even though the SC is very stable as seen in the Fig. 5(a) power spectrum time series. The RMS-N and Φ_{RSN} of the laser seed was 0.6% and 1% respectively, over the 45 minute measurement interval (and is typical for all subsequent

#179077 - $15.00 USD Received 1 Nov 2012; accepted 2 May 2013; published 24 May 2013

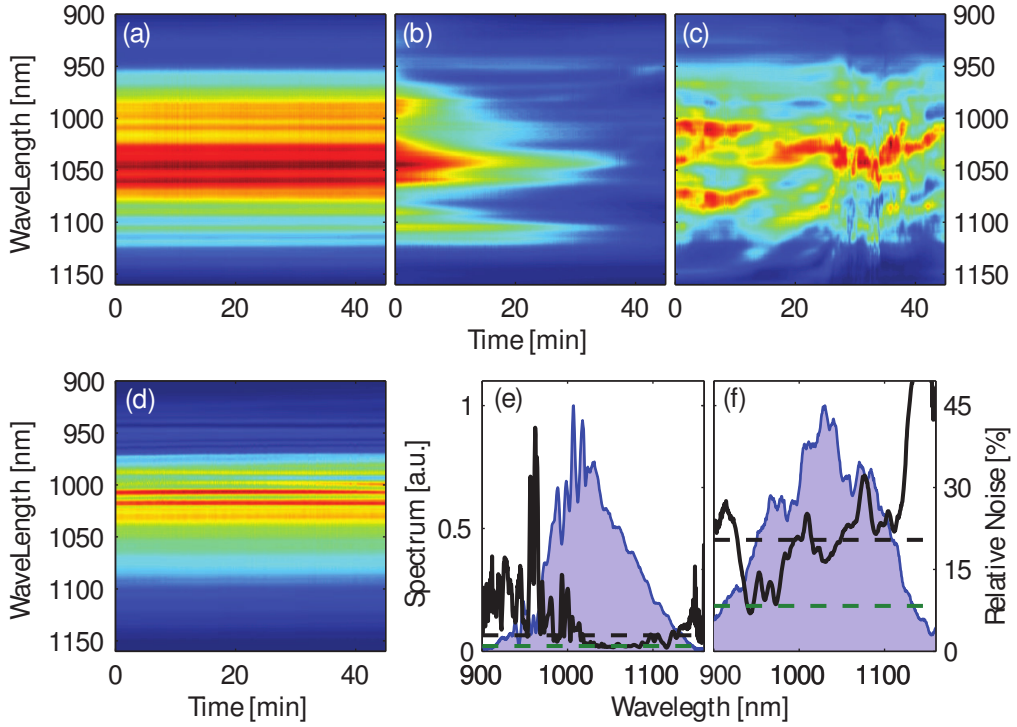

Fig. 5. SC time series for (a) 200 mW, (b) 300 mW, (c) 375 mW, and (d) 300 mW (after 4.5 hours of fiber warm-up) coupled power in UHNA-3 fiber. The mean power spectrum (shaded blue), RSN (solid black), Φ_{RSN} (dashed black), and RMS-N (dashed-green) in (e) and (f) from the time series (d) and (c), respectively.

measurements). The seed RSN is smooth across the spectrum, free of any spectral mode shape changes. The SC RMS-N is 1% over the 45 minute time interval, just above the seed noise. The Φ_{RSN} is in close agreement to the RMS-N at 1.5%, indicating a high spectral stability.

Above 200 mW, the SC is subject to extremely long thermal equilibration times. At 300 mW, the total integrated power decays (nearly linearly) through the first 45 minute measurement; losing 75% of the polarized coupled power to the orthogonal mode, shown in Fig. 5(b). The RMS-N for the 45 minute interval would therefore be huge, but less meaningful since it would just be a measure of warm-up dynamics not an equilibrium stability. After 4.25 hours of warm-up and re-tuning the exit waveplates, the SC has improved from the decaying time series of Fig. 5(b) to Fig. 5(d). Not only is the SC more stable but the mean power spectrum in Fig. 5(e) also takes on the roughly triangular form expected from the GNLSE propagator. The depolarization settles to 27% and the RMS-N stabilizes to 1% for both 1 and 45 minute intervals. The RSN for 1 minute intervals is $\sim 3\times$ less at the peaks than for the full 45 minute interval. While the long time interval RSN has large features (solid black line in Fig. 5(e)), the large RSN fluctuations ($> 10\%$) are isolated to regions of low power spectral density as evidenced by the small Φ_{RSN} at 1% and 3% for 1 and 45 minute measurements respectively. The small difference in RSN-N and Φ_{RSN}, dashed green and black lines in Fig. 5(e) respectively, indicates a maintained spectral stability after sufficient thermalization.

At 375 mW there appears to be a phase change, as seen in the Fig. 5(c) power spectrum time series. Above this threshold, spectral components continuously drift between the orthogonal

#179077 - $15.00 USD Received 1 Nov 2012; accepted 2 May 2013; published 24 May 2013

polarization modes and do not stabilize, even on timescales of many hours. The spectral fluctuations are highly co-/anti-correlated across the spectrum, resulting in the rough preservation of the total integrated power in the output polarization mode. The RMS-N averages only 1% for any 1 minute interval and 8% for the full 45 minutes, dashed green line in Fig. 5(f). The depolarization is around 50%, fluctuating with the RMS-N. The RSN is everywhere higher for the either 1 or 45 (solid black line in Fig. 5(f)) minute intervals. The Φ_{RSN} is also markedly higher than the RMS-N at 3% and 20% for 1 and 45 (dashed black line in Fig. 5(f)) minute time intervals, respectively.

In this unstable regime, measurements of the full beam on a photodiode would be an inadequate measure of the SC stability. Significant amounts of spectral noise are masked by the highly correlated nature of the spectral fluctuations, as seen in the $2.5\times$ higher Φ_{RSN} over the 45 minutes interval compared to the RMS-N. Shorter time-scale measurements of stability are also misleading as the RSN, Φ_{RSN}, and RMS-N are dramatically lower for short time windows. In contrast with the 300 mW case, this is not a thermal relaxation issue. We measured spectra for 4.5 hours without ever seeing a change from the continuously evolving spectra of Fig. 5(c).

Our experiments also indicate that this instability threshold is not explainable as fiber degradation. The same fiber repeatedly returns to the same spectra below threshold after prolonged pumping above threshold. Also the highest coupled average powers are well below the damage threshold reported for these fibers in Ref [17]. This destabilization transition sets a sharp limit on the power that can be used for a SC-broadened source. In order to scale to higher average power SC sources with normal dispersion fibers, a larger and more stable fiber birefringence is required.

3.2. Strongly birefringent nonlinear fiber

In strongly birefringent fibers, the large contrast in orthogonal indices of refraction eliminates the phase-matching condition that gives rise to the polarization modulation instability. While attempts have been made to induce birefringence through high stress levels [6, 18], the optimal solution is PM, all normal dispersion, nonlinear fiber. In the absence of such a PM nonlinear fiber, one can potentially induce enough asymmetrical strain in the fiber to create strong birefringence. Tu et al used a pinch plate along a 27 cm length of PCF fiber and largely eliminated the polarization modulation instability defects from the measured power spectrum and reduced the depolarization from 60% to 20% [6]. For fibers where longer lengths and WB are desired, a small expandable spool could be employed. We found mixed results with this strategy using 1 m of UHNA-3 wrapped onto a 12 mm diameter spool and $2-4\%$ strain. We were able to reduce the depolarization from 26% to 20% at 300 mW average power, in comparison to Figs. 5(d) and 5(e). It was unclear however, if this was not purely a result of thermal relaxation after significant fiber warm up time.

Fibers with designed high birefringence disallow polarization modulation instability and therefore polarization instabilities for seeds aligned to the slow axis. The polarization eigneaxes of such a PM fiber are also insensitive to the environmental perturbation seen in stress induced birefringent fibers: thermal relaxation and long-term strain relaxation. CorActive offers a suitable, commercially available, UHNA PM-nonlinear fiber: SCF-UN-3/125-25-PM. Theoretically, the strong birefringence should eliminate polarization modulation instability; however, a direct comparison between the CorActive and Nufern fibers is limited by the fact that the CorActive fiber nonlinearity is 40% of the Nufern value, due to the lower confinement in the larger CorActive core.

We tested the SC stability from the CorActive PM UHNA fiber with a long fiber cocktail: 12 mm Panda-type fiber and 2 m of nonlinear PM fiber. At 375 mW average power coupled into the PM nonlinear fiber cocktail, the SC depolarization is 10% and required no thermal

#179077 - $15.00 USD Received 1 Nov 2012; accepted 2 May 2013; published 24 May 2013

equilibration time. The stable time series is shown in Fig. 6(a). The RMS-N averages 0.3% over any 1 minute interval and 0.7% for the full 45 minute measurement (Fig. 6(b) dashed green line). The RSN (Fig. 6(b) solid black line) is $< 1\%$ across the power spectrum for both 1 and 45 minute intervals, and the Φ_{RSN} is close to the RMS-N at 0.5% and 0.8% for 1 and 45 minute (Fig. 6(b) dashed black line) intervals respectively, a marked improvement over the SC from the non-PM UHNA fiber.

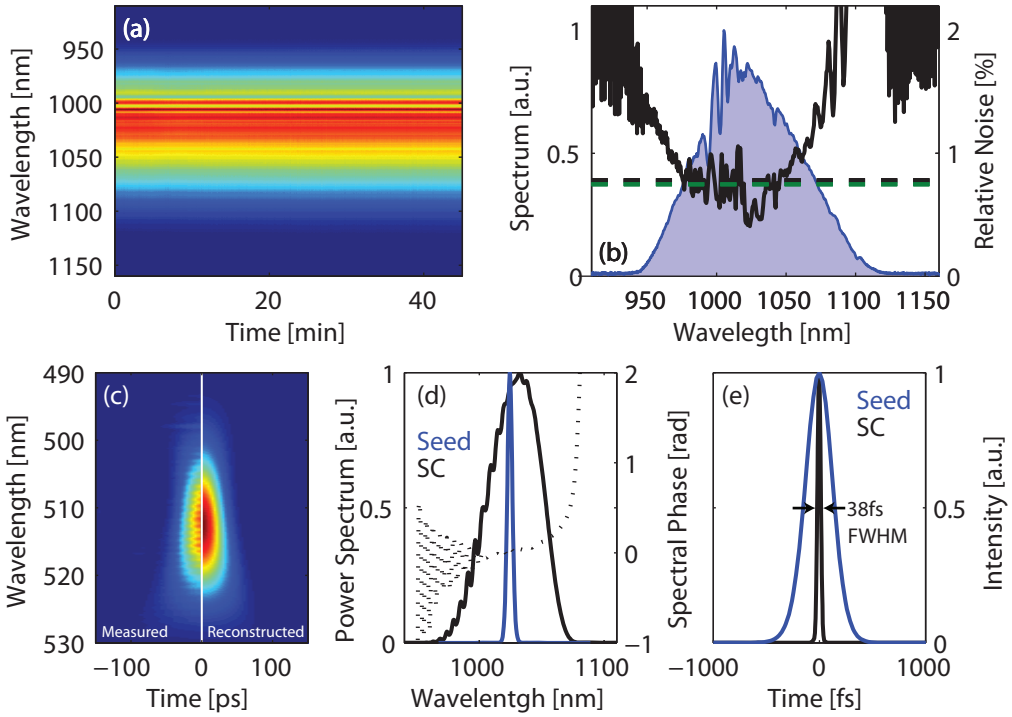

Fig. 6. SC time series (a) and (b) power spectrum (blue), RSN (solid black), Φ_{RSN} (dashed black), and RMS-N (dashed-green) for the 45 minute time interval in (a) from 375 mW average coupled power into CorActive PM UHNA fiber. The Phantom SHG-FROG (c), the SC reconstructed power spectrum (black) and spectral phase (dashed-black), and seed power spectrum (blue) in (d). The normalized seed intensity (blue) and the reconstructed SC intensity after a two stage compression system (e).

3.3. Nonlinear pulse compression

In the remainder of the paper, we make use of a shorter fiber cocktail which we will refer to as the short pulse fiber. This fiber system contains 12 mm Panda-type entrance fiber, 25 cm of CorActives PM nonlinear fiber, followed by 13 mm of a custom Nufern PM fiber similar to UHNA-4. The custom Nufern PM fiber had the appropriate cladding size for APC connectorization and minimized bandwidth losses at the splice compared to standard core-sized PM fibers (the CorActive cladding is unfortunately just over the standard 125 microns). The length of nonlinear fiber is much greater than the WB threshold, determined experimentally by the presence of WB/FWM sidebands in the power spectrum measured directly out of the fiber (not shown). We were unable however, to obtain specific dispersion data for the CorActive fiber to calculate the length for the onset of WB. The fiber length was kept short to aid in pulse compression by reducing the opportunity for a broad spectrum to sample the fiber dispersion map.

#179077 - $15.00 USD Received 1 Nov 2012; accepted 2 May 2013; published 24 May 2013

The total transmission of the short pulse fiber is 48%, with 50% coupling efficiency into the nonlinear fiber.

One of the primary goals of nonlinear fiber broadening is the production of compressed pulses much shorter than the seed pulse, which more effectively drive nonlinear optical interactions. As discussed earlier, nonlinear fibers with sufficient length for WB require a pulse shaper to completely compensate the complex spectral phase. For our particular short pulse fiber, the large dispersion overwhelms the dynamic range of our spatial light modulator (SLM), so we added a grating compressor to the output of a 4-F pulse shaper. The pulse shaper was calibrated using the in-line spectral interferometry technique [19]. As our modulator is designed and coated for operation in the Ti:sapphire spectral region, we suffer from a thin-film dispersion resonance in the AR coating of the modulator in the region of 1050 nm. Errors in the calibration of the shaper response, introduced by the thin-film coating resonances, prevented a direct inversion of the spectral phase recovered from an SHG-FROG reconstruction to quickly obtain transform limited pulses, as is possible when the resonances are absent.

With most of the GDD eliminated by the grating compressor, an SHG-FROG measurement determined an initial phase mask to apply to the pulse shaper. We then used a simple genetic algorithm to improve the 2π-wrapping points and secondarily too improve the shape of the phase mask itself. The resulting pulse is shown in Figs. 6(c)-6(e), with remnants of the 2π-wrapping point error seen in the power spectrum and spectral phase of Fig. 6(d).

The power spectrum directly out of the fiber, potentially supporting a 20 fs pulse, is broader than the spectra we reconstruct from SHG-FROG. Two major contributing factors to the spectra loss are spatial chirp from the pulse shaper and wavefront error introduced by the SLM modulator. The SLM is a 2005 model Cambridge Research Inc 640 pixel unit, that exhibits a wavefront error of $> 3\lambda$ when double passed. The combination of errors kept our system from delivering the full bandwidth out of the fiber to the focus of the SHG-FROG. The spectral loss is not due to phase-matching limitations in the Type-I KDP crystal, as we previously measured broader bandwidth SC with the SHG-FROG apparatus (e.g. see Fig. 4). Even with the lost power spectral wings, the reconstructed pulse, with 0.004 FROG error, is 37.6 fs FWHM, compared to a bandwidth supported transform-limit of 36 fs FWHM. The $9\times$ compression ratio is shown in Fig. 6(e). Changing the architecture to minimize the spectral/spatial aberrations will enable the utilization of longer fibers for still shorter pulses. Longer fiber cocktails were made, but were limited to temporal pulses and bandwidths above those supported by the fiber cocktail due to spectral losses through the compression system. SHG-FROG is an excellent means of characterizing pulses for this reason, it demonstrates the actual spectral bandwidth one might deliver to the focus of a nonlinear experiment.

4. ANDi Seeded Supercontinuum

4.1. Nonlinear propagation of ANDi seed pulse

Yb-doped ANDi fiber lasers are an attractive alternative to traditional soliton-like modelocked oscillators, due to their simplicity in construction, low cost, and high spatial mode quality in addition to their scalability in bandwidth and pulse energy. While they are a compelling seed source for SC generation, ANDi lasers are not a direct stand-in for the bulk Yb:KYW (soliton-like) seed pulses. The dissipative-soliton pulses from the ANDi laser have characteristic "cat-ears" in the power spectrum, Fig. 7(a) contains a representative power spectrum obtained through an SHG-FROG reconstruction. The cat-ears contribute to a SC power spectrum with much higher structure than that seen from sech pulses, even in the case of a transform limited ANDi seed pulse.

It is unfortunate, if not surprising, that ultrafast pulses derived from a fiber source in the 1 μm region require HOD dispersion compensation for clean short pulses. The SC dispersion

#179077 - $15.00 USD Received 1 Nov 2012; accepted 2 May 2013; published 24 May 2013

dynamics developed earlier in this paper are helpful in explaining why a simple compressor is insufficient. The ANDi pulses come out of the oscillator at ~ 5 ps FWHM, so their accumulated dispersion is at least > 1 and the ~ 100 fs transform limit supported bandwidth is sufficient to sample the HOD of the fiber. Figure 7(b) shows ANDi seed pulses with increasing polynomial orders of spectral phase compensation, demonstrating the necessity for HOD compensation to realize a true short pulse with minimum pedestal. Indeed the peak power with GDD and TOD compensation is only 50% of that possible from the transform limit. Compensating up to fourth order dispersion (FOD) brings the FWHM to 118 fs and the peak power to within 87% of that possible from the 113 fs transform limited case.

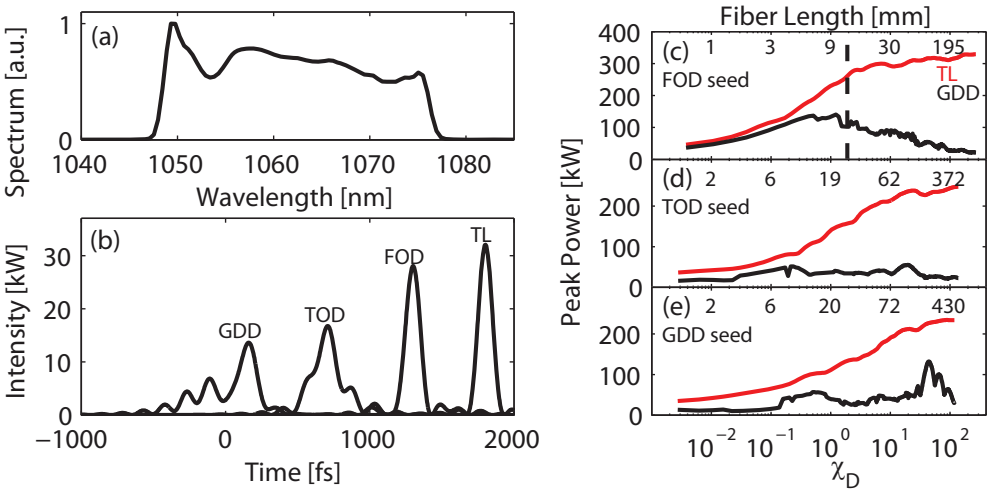

Fig. 7. The power spectrum (a) and intensity, labeled GDD, (b) of the ANDi seed pulse reconstructed with SHG-FROG. Also in (b) are ANDi pulse intensities with up to TOD and FOD spectral phase compensation along with the transform limit. The peak power evolution with χ_D of SC with GDD compensation (black) and the transform limited SC (red) for some of the ANDi seed pulses in (b): FOD (c), TOD (d), and GDD (e). The onset of WB is plotted in (c) as a dashed vertical line.

By seeding the fiber propagator with the ANDi pulses in Fig. 7(b), we seek to understand how the ANDi seed pulses compare to the simpler sech seed pulses. With FOD compensation, the SC evolution process is quite close to the sech cases studied previously, as seen in Fig. 7(c). The peak power enhancement with only GDD compensation of the SC for a FOD compensated ANDi seed pulse occurs with less accumulated dispersion than the SC from a comparable transform limited sech pulse, e.g. compare Fig. 7(c) to Fig. 2(a). The slight reduction in the location of the peak enhancement is due to the residual HOD on the incident ANDi seed pulse.

The peak power with compensation below FOD, results in an overall reduction in generated SC bandwidths, shown in Figs. 7(d) and 7(e). The transform limit of the produced SC is comparable to that produced by a ~ 250 fs sech seed pulse of equivalent energy, e.g. compare Figs. 7(d) and 7(e) to Figs. 2(b) and 2(c). However, the SC from GDD and TOD compensated ANDi seed pulses experience virtually no peak enhancement effects. For the optimal case of seed pulses with FOD compensation, the residual HOD interrupts the compressibility of the SC generated primarily by SPM sooner than in the idealized case of a transform-limited sech seed pulse. For seed pulses with less than FOD compensation, the residual HOD (now including FOD) is sufficient to immediately shut down the SC's compressibility with only GDD compensation. Even though the accumulated dispersion length is defined in terms of GDD, it is

#179077 - $15.00 USD Received 1 Nov 2012; accepted 2 May 2013; published 24 May 2013

reasonable to think about the ANDi seed pulses as having $\chi_D > 0$ at the start of the fiber. It then follows that the peak enhancement should shifts to ever shorter fiber lengths with increasing incident accumulated dispersion (increasing incident residual HOD). At the extreme, the peak enhancement vanishes, and the SC requires HOD compensation for any fiber length to produce short pulses.

4.2. ANDi seed pulses in strongly birefringent fiber

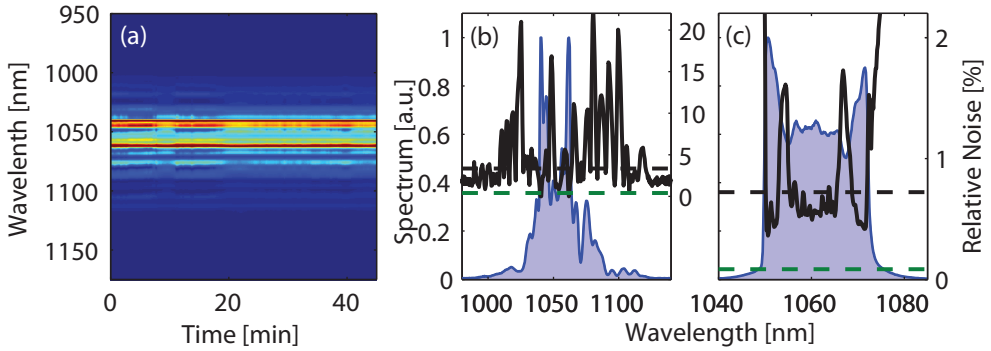

Fig. 8. SC time series (a) and mean power spectrum (shaded blue), RSN (solid-black), Φ_{RSN} (dashed-black), and RMS-N (dashed-green) (b) from 45 minute time intervals from ANDi seeds and 190 mW couple power. (c) The ANDi oscillator mean power spectrum (shaded blue), RSN (solid-black), Φ_{RSN} (dashed-black), and RMS-N (dashed-green)

The increased role of incident spectral phase for ANDi seed pulses aside, it is still necessary to produce stable SC for application, whatever dispersion complexities must be overcome. We tested SC stability from the short pulse fiber, seeding with pulses from an ANDi laser which pass through a grating compressor prior to entering the fiber (shown in Fig. 7(b) GDD). We coupled 190 mW through the short pulse fiber cocktail with only 2% depolarization and 49% total fiber efficiency. The resulting SC power spectra, Figs. 8(a) and 8(b), are marked by the residual tall cat-ears of the seed pulse. The integration time of the spectrometer was long enough to saturate the cat-ears, improving the signal-to-noise of the the low power WB/FWM spectral wings. The blue and red cat-ears saturated only 1 and 2 pixels of the spectrometer respectively (0.5 nm and 1 nm).

The seed pulses from the ANDi laser are less noisy than the Yb:KYW seed pulses used elsewhere in this paper: RMS-N of 0.08% and Φ_{RSN} of 0.7%, as seen in the dashed lines of Fig. 8(c). While these noise metrics are low, the RSN contains two relatively large features, RSN(1054 and 1067 nm) $\sim$ 1.5%, just inside of the cat-ears which indicate noise dynamics more subtle than just fluctuations in total seed power. The SC RMS-N is also very low averaging 0.08% for 1 minute intervals and increases to only 0.2% for the full 45 minute interval, dashed green in Fig. 8(b). The SC's RSN however, is as high as 23% for the full 45 minutes (solid line in Fig. 8(b)). The relatively low Φ_{RSN} at 0.8% and 3.4% at 1 and 45 (Fig. 8(b) dashed black line) minute intervals respectively, show the spectral fluctuations are concentrated in, if not limited to, areas of low power spectral density.

The ANDi undergoes small spectral mode shifts, the aforementioned 1.5% fluctuations at the inside of the cat-ears, which map to large changes in the SC power spectrum. The mode changes are visible in the SC time series, e.g. see around 10 minutes of the time series shown in Fig. 8(a). The mapping of small changes in the shape of the seed power spectrum, but practically

#179077 - $15.00 USD Received 1 Nov 2012; accepted 2 May 2013; published 24 May 2013

no total seed power fluctuations, to large changes in the output power spectrum is characteristic of a cascaded nonlinear process. Reducing these already small seed spectral mode fluctuations will be necessary to improve the SC generated from ANDi seed pulses.

5. Conclusion

The introduction of the local and accumulated dispersion/nonlinear lengths have become valuable tools for us in designing nonlinear fiber cocktails and interpreting SC spectral phase. The accumulated dispersion length, in particular, provides a simple explanation for the necessity of a pulse shaper to compress SC generated in fibers with WB. The full study of the spectral phase evolution will serve as a guide for the future design of fiber cocktails.

We identify a polarization instability in the generation of SC in weakly birefringent, all normal dispersion, UHNA fiber. Unlike previous work regarding polarization modulation instability, we focus on the temporal dynamics of the instability. We report an instability power threshold, above which, the output SC's spectral polarization state is seeded from noise. Large fluctuations in power spectral density within the analyzed output polarization are highly correlated which masks the magnitude of the spectral instability when characterized by the total integrated power.

The use of a PM, all normal dispersion, UHNA fiber eliminates the spectral instability when seed pulses are oriented along the slow axis of the fiber. The resulting stable SC is compressed using a two-stage compression system, composed of a 4-F pulse shaper in conjunction with a grating compressor to compensate for the HOD and large GDD respectively. The polarized output of the short pulse fiber and tiered compression system is a near transform limited 37.6 fs pulse.

SC evolution and spectral stability from an ANDi-type laser is also presented. Our results demonstrate the heightened complexity required to properly prepare an ANDi seed pulse for ideal SC generation. The SC spectral stability is promising, but also illustrates the mapping of small spectral mode shape noise to large SC spectral mode fluctuations through a cascaded nonlinear process, the otherwise negligible integrated seed power noise not withstanding.

Acknowledgments

S.R. Domingue and R.A. Bartels are grateful for support from grant number **1R21EB011717** from the National Institutes of Health and grant number **DE-SC0001559** from the Department of Energy. The authors are also grateful to David Winters for his extensive intellectual and technical collaboration.

#179077 - $15.00 USD Received 1 Nov 2012; accepted 2 May 2013; published 24 May 2013